LA-UR- 04-6065

Approved for public release; distribution is unlimited.

Title: Alloy Synthesis Using the Mach Stem Region in an Axial Symmetric Implosive Shock: Understanding the Pressure-Strain-Temperature Contributions

Author(s): Karl P. Staudhammer

Submitted to: International Symposium: Peter Salcher and Ernst Mach - A Successful Teamwork, Rijeka, Croatia
September 23-25, 2004

Alloy Synthesis Using the Mach Stem Region in an Axial Symmetric Implosive Shock: Understanding the Pressure-Strain-Temperature Contributions

Karl P. Staudhammer
Los Alamos National Laboratory, Nuclear Materials Technology Division, PO Box 1663, MS E 504, Los Alamos, New Mexico, 87545, U. S. A.
Phone 505-667-9333, FAX 505-665-7895, staudhammer@lanl.gov

Abstract: *The Mach stem region in an axial symmetric shock implosion has generally been avoided in the dynamic consolidation of powders for a number of reasons. The prime reason being that the convergence of the shock waves in the cylindrical axis produce enormous pressures and concomitant temperatures that have melted tungsten. This shock wave convergence consequently results in a discontinuity in the hydro-code calculations. Dynamic deformation experiments on gold plated 304L stainless steel powders were undertaken. These experiments utilized pressures of 0.08 to 1.0 Mbar and contained a symmetric radial melt region along the central axis of the sample holder. To understand the role of deformation in a porous material, the pressure, and temperature as well as the deformation heat and associated defects must be accounted for. When the added heat of consolidation deformation exceeds the melt temperature of the 304 powders, a melt zone results that can consume large regions of the compact while still under the high-pressure pulse. As the shock wave traverses the sample and is removed in a momentum trap, its pressure/temperature are quenched. It is within this region that very high diffusion/alloying occurs and has been observed in the gold plated powders. Anomalous increases of gold diffusion into 304 stainless steel have been observed via optical microscopy, scanning electron microscopy and EDAX measurements. Values exceeding 1200 m/sec have been measured and correlated to the powder sizes, size distribution and packing density, concomitant with sample container strains ranging from 2.0% to 26%.*

Key words: Shock consolidation, Shock melting, Strain heating, Shock adiabate, Shock quenching, Axisymetrical Implosion, Momentum trapping,

1. INTRODUCTION

Much research within the metallurgical community has been devoted to developing new alloys. Traditionally, alloy development entailed the mixing of two or more elements usually in the liquid state, as at high temperatures all the elements are miscible in one another. When solidified the resultant solid contains changes in structure and properties. Generally, this entailed a sequence of processes in alloying and systematic evaluations. For the most part the evaluations looked for beneficial properties in strength, hardness, electrical, magnetic, corrosion resistance, etc.; it was and still is indeed a tedious process. Also sought, was stability in the alloy being developed in its manufacture and its service life. Not until recently with few exceptions, manufacturing processes over the past several decades have investigated other non traditional manufacturing processes such as splat cooling and rapid solidification to obtain non equilibrium states that are meta stable at lower temperatures for significant periods of time. Indeed many such alloy materials proved to have unique properties when utilized within their temperature range. While this research has demonstrated that unique and potentially useful

materials can result when liquid metals are subjected to cooling rates in excess of 10^4 K/sec., methods to satisfactorily consolidate such materials into useful monoliths without destroying the unique qualities of the powder in the process, have been lacking. Obviously, conventional sintering or hot pressing subjects the powders to temperature extremes that can be unacceptable. Among the alternative methods, dynamic, or shock wave, consolidation is unique in that it offers the possibility of producing the high temperatures necessary for adequate metallurgical bonding precisely where they are required—at the powder particle interfaces—while the remainder of the powder mass remains relatively cool. Thus, thermally induced Microstructural changes in the bulk of the powder can be minimized.

In shock compression of powders an unusual combination of material characteristics can significantly promote physical and chemical reactivity's of powders and lead to accelerated mass transport kinetics. Under such unique conditions, not only can metal and other materials be dynamically consolidated [1-3], or undergo solid-state phase transformations [4-8], including chemical reactions and molecular decomposition of compounds in powder mixtures [9-12], resulting in synthesis of compounds and alloys have also been observed. This process not only encompasses rapid heating and cooling, but also that it can occur under pressure with the possibility of pressure quenching.

Chemical reactions occurring in mixtures of elemental or alloy powders are often accompanied by rapid release of large amounts of energy. The energy release, unlike that in detonation of explosives, is generally manifested by the generation of high temperatures, often exceeding the melting temperature of the reaction products. Such high-rate chemical reactions can be advantageously utilized to synthesize materials with novel phases and unique microstructures, or to generate radically modified materials with physically interesting or technologically useful properties [11]. This type of synthesis technique is referred to as "Shock Synthesis". If the time scale of the shock event (usually in the nano to microsecond range) is faster or ahead of the reaction kinetics of the materials being investigated, then the process is referred to as "Shock-Induced Reaction Synthesis". Also, by studying the chemical effects associated with shock synthesis and shock-induced reaction synthesis, an improved fundamental understanding of shock-compression phenomenon can be obtained.

The fundamental processes that control shock-induced reactions in powder mixtures leading to synthesis of compounds and alloys are dominated by conditions prevailing during nano/microsecond-scale duration of the high pressure, stress/strain, strain-rate, and temperature states. However, at the present time, no generally accepted theory is available to account for the process mechanisms, threshold conditions for reaction initiation, and the rapid-reaction kinetics. Thus, occurrence of high-rate chemical reactions by usual mechanisms, namely, formation and growth of nuclei, either from the molten "liquid", or by diffusion in the "solid" state, is not possible during shock-compression, because of kinetic limitations. For this and other reasons "Shock Synthesis" has been predominantly limited to reaction kinetics involving exothermic reactions and for the most part are really "Shock-Induced Reaction Synthesis". This is evident from the fact that an initiated reaction by a shock wave continues even for several minutes after the passage of the shock wave.

On a parallel path of shock consolidation work throughout the past several decades, the goal was to shock compact powders into solid homogeneous full density units with little or no melting of the constituents. Consolidation was the primary objective. However, as the multitude of parameters and variables were not and in many cases still is not fully understood, over (as well as under) compaction resulted in many experiments. For the under compaction insufficient

energy produced some compaction, but did not yield consolidation with sufficient particle-to-particle bonding. On the other hand over compaction resulted in excess energy deposition in the system and the particles melted, thus loosing the intent of the original powder Process. As a result, much of the shock compaction work revolved around achieving the optimal shock conditions to just "weld" the particle surfaces together and no more. Results for planar shock compression, due to geometric considerations were quite different than those for radial-axial implosions. The radial-axial implosion techniques when over compacted contain a melted region through the central axis. This melted region results from the radial convergence of the shock wave as it travels in and down the length of a cylindrical sample, and is called the Mach stem. In this region the pressure and temperature are maximum within a given sample. If one now considers powder consolidation, the added strain from void collapse and its resulting strain heat being added can generate extraordinary conditions of temperature and pressure. It is this Mach stem that many investigators have tried to eliminate and avoid. What is so unique within this Mach stem is that it affords us the opportunity to do research in the pressure-temperature arena here-to for unachievable by any static conditions. Utilization of this axisymetrical implosion design has as its main advantage the ability to provide in one experiment a range of pressures, temperatures, strains and reaction kinetics. It is a very powerful screening technique to investigate a large number of variables within the shock event.
In this paper, I will present a different way of viewing the shock process that will show the interdependence of the shock wave and its magnitude, the powder size and distribution, strain deformation and the associated temperature within the shock event toward synthesis.

2. THE SHOCK PULSE

It is not the intent of this paper to develop the concepts of shock wave generation or its definitive parameters. Numerous resource articles detailing the generation and understanding of this are in the literature at large (13,14). However, a basic understanding of the shock event as depicted in figure 1 is appropriate. As a shock wave propagates through a solid material as a shock front it separates the material into two regimes: deformed and undeformed, and in between, this shock front has a finite thickness. In the high-pressure region behind the shock front, the material is compressed. Consequently, the regions in front of and behind the shock front have different densities (ρ_o, ρ), specific volumes (V_o, V), internal energies (E_o, E) and pressures (P_o, P), the shock front velocity is designated by U_s and the particle velocity by U_P which is equal to zero in front of the shock wave but greater than zero behind the shock front. Considering the conservation of mass, energy and momentum across the shock pulse leads directly to the Rankine-Hugoniot relationships, using:

$$U_p - U_o = U_s(1 - V/V_o) \qquad \text{Mass conservation} \qquad (1)$$

$$P - P_o = (Us/V_o)(U_p - U_o) \qquad \text{Momentum conservation} \qquad (2)$$

$$E - E_o = (1/2)(P + P_o)(V_o - V) \qquad \text{Energy conservation} \qquad (3)$$

Thus, given any two of the variables, these equations can be used to obtain the others. In effect these equations of states relate volume with pressure, and for given values of P_o, ρ_o and V_o in

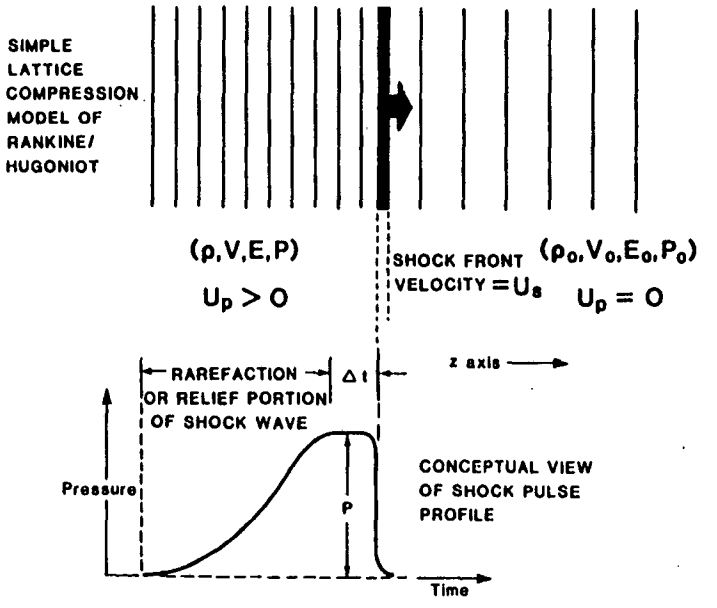

Figure 1. Schematic representation of two states of condensed matter ahead of and behind a propagating shock-wave pulse. The undisturbed region ahead of the shock front is characterized by density ρ_o, volume V_o, internal energy E_o, and pressure P_o, and a particle velocity, $U_p = 0$. Behind the shock front, the particle velocity is related to the mean peak shock pressure.

the uncompressed material ahead of a shock front, allows a relationship between P, ρ, and V in the compressed region behind the shock front to be established. Resultantly, a pressure-density or pressure-volume relationship is often called the Rankine-Hugoniot equation or simple the Hugoniot. This equation represents the loci of all P, V states which can be obtained by shock compression of a solid material from an initial P_o, V_o state. This is schematically shown in figure 2a for explosive compression of a solid material. Thus, the energy imparted to the shocked material at pressure P_1 is the area under the P_1 V_1 V_o curve. Upon release of the shock wave, the pressure returns to P_o and the volume returns to V_o along the release adiabate. The area below the release adiabate is equivalent to the adiabatic temperature and is only present under the pressure pulse. The area above the release adiabate is equivalent to the residual temperature left behind in the sample. Empirical data used in determining the Hugoniot curves for a host of metals and other materials have been published by [15] and more recently by [16] where they have developed a series of Hugoniot tables relating P-V data for a number of materials based on computer solutions using the equations cited above. However, for, porous materials, such as that depicted in figure 2b, the same phenomena occurs except that the distended material will have a loss of porosity and an increase in density. That is to say that upon release of the shock wave the release adiabate will return to the new compacted volume. Thus the deposited energy into the distended material will have a much larger residual component. The area under the curve defined by $P_1V'_E$ and V'_o depicts this. The loss of this porosity and its concomitant energy results in an increase of internal energy, i.e., an increase in residual temperature. It is in understanding the magnitude of this temperature and its source distribution that better consolidation of powdered materials is obtained, as well as greater control for shock synthesis and alloying. There are many system designs for producing shock conditions. The one utilized for the work discussed in this paper is an axisymetric implosion

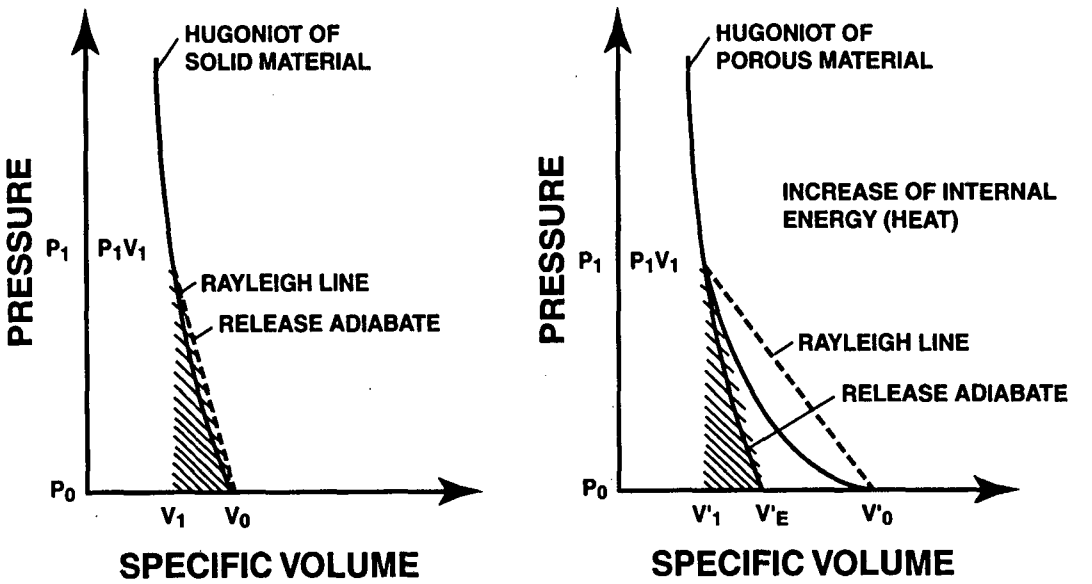

Figure 2. Pressure volume relationships for the explosive compaction/consolidation of powdered materials a) solids and b) distended materials.

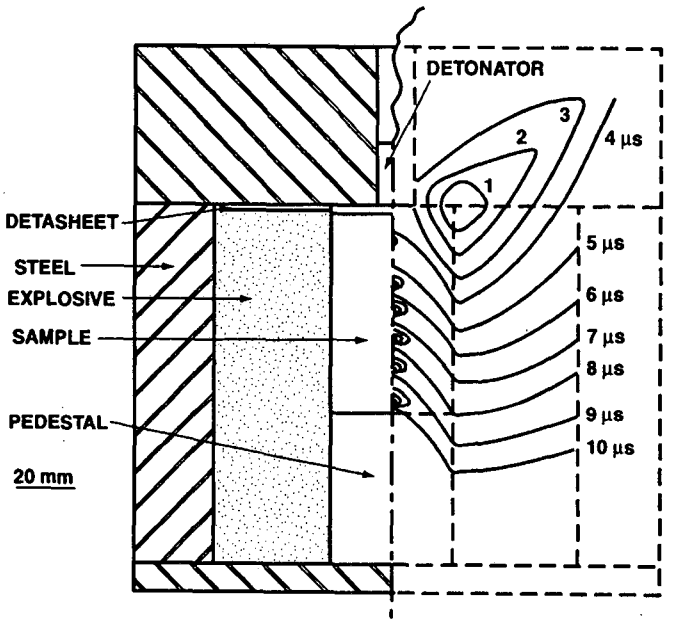

Figure 3. Schematic of shock loading assembly showing pressure-time contours of the shock wave.

design developed at Los Alamos National Laboratory and is shown in figure 3 and extensively described elsewhere [16]. One must also keep in mind that a shock pulse generally has a duration of 0.1 to 1 μsec, though higher durations can be achieved. Because this pulse duration and pulse time is so short, unique opportunities exist in utilizing the associated temperatures within and after the shock event. These are present below.

2.1. High Rate Deformation

We need to emphasize that we are dealing with dynamic phenomena that are produced by shock waves, which can result in a high rate of deformation. Thus if a shock wave from an explosion or an impact produces some deformation (strain) of a material, the rate at which this straining will occur, will quite logically be very high relative to that which occurs when a simple Uniaxial powder compression process is performed. At sufficiently high pressures where a solid is stressed beyond its elastic limit (even in the case of Uniaxial compressive shock waves), the deformation is considered to be ideally hydrostatic. Thus, the three principle stresses are essentially equal and thus experience a uniform deformation. While this is a convenient assumption in dealing with compressibility in ideal solids, it is unrealistic in dealing with plastic deformation in a solid, and even more so for metal powders. It is generally observed that the flow stress and strain rates are related and the sensitivity of solid, crystalline materials to strain rate varies considerably. It can also vary considerably when defined as a function of flow stress or yield stress as shown by [17]. This phenomenon is defined as strain rate sensitivity and varies with a change in stress with respect to a change in the logarithm of strain rate at constant strain. For many metals and alloys, the strain rate sensitivity does not change appreciatively for strain rates up to about $10^3 s^{-1}$. However, above 10^4 the strain rate sensitivity can change significantly. Also, strain magnitude can have an influence as well as strain state. Johnson et al. [18] has shown that in the case of type 304 stainless steel, Martensite volume fraction corresponding to specific strain levels is very significantly influenced not only by strain rate, but also by strain state. Consequently we need to understand the strain effects at these high rates as they do contribute and influence temperature in a major way.

2.2. Strain Effects

In utilizing shock waves there are two major components of strain associated with the shock event on metal powders. They are the overall strain of the sample holder and the local strain associated with the collapse of the distended powder. Both of which can be extensive, but controlled. The degree and type of momentum trapping of the shock wave govern the overall strain associated with the shock event. In 304 stainless steel samples this strain can be controlled between about 1.9% to Spallation fracture (>25%). The observations of these experiments were reported earlier in [19], and are shown in figure 4. These strain values were obtained experimentally by a split solid sample that had circle grids electroplated on its central surface. This is shown for a post-shocked Inconel 625 sample in figure 5. The strain data from such samples are given in figure 6 for 304 stainless steel. This overall strain is significant in powder consolidation; shock synthesis and alloying in that low overall strains are needed to produce solid crack free compacts. Now this is well understood and utilized in shock work. The second major strain effect comes from the deformation of the powder as it is being compacted. This powder deformation strain is of course a strong function of many other parameters such as original packing density, powder size and distribution, and powder morphology. It is from this realm that a large contribution is derived for synthesis and alloying, especially with in the Mach stem region. These aspects will be discussed in more detail particularly as they pertain to the resulting temperature effects.

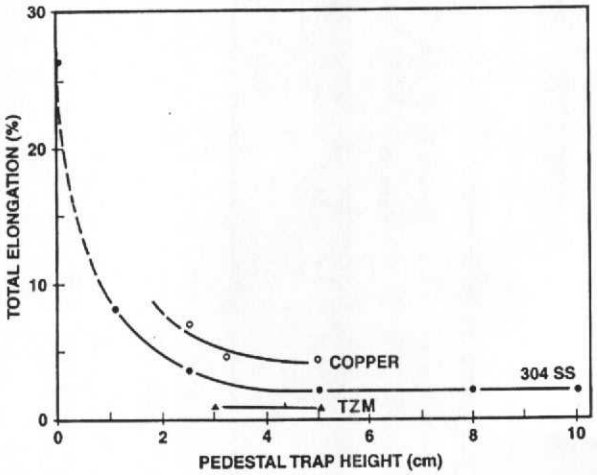

Figure 4. Total elongation versus pedestal height for 304 stainless steel, copper and TZM in an axisymmetric shock loading assembly.

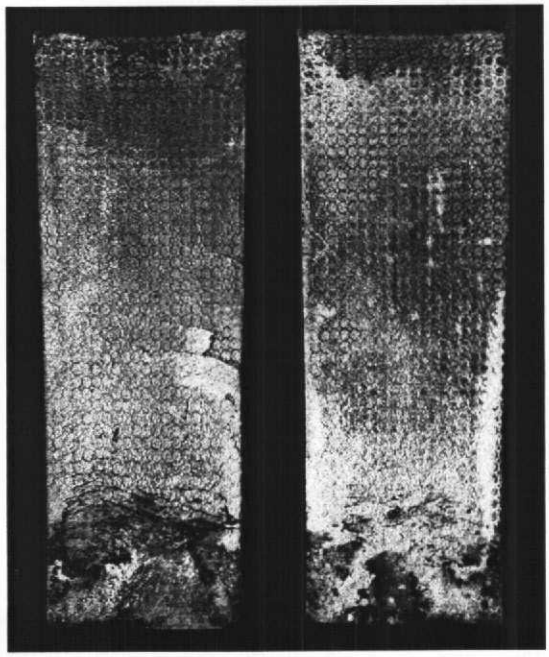

Figure 5. Post shock anvil surface of Inconel 625 alloy. Copper electroplated circle grids had an initial diameter of 1.27 mm (0.050 inches). Sample length, 6.7 cm.

2.3. Temperature Effects

There are five temperature contributions involved in a shock event pertinent to consolidation, shock synthesis and alloying. Three of which result from the shock event in non-reactive material systems. The additional two temperatures are the initial pre shock temperature, T_o and if dealing with reactive powder components, a chemical or metallurgical endothermic or exothermic reaction, resulting in a change in the net temperature, $\Delta T_{reaction}$. These are schematically shown in figure 7. For the consolidation of metal powders, the $\Delta T_{reaction}$ component generally is not present. Thus, the three major shock temperatures are described as, 1) the adiabatic temperature rise, ΔT_A, resulting from the shock event and is a strong function of the shock pressure. 2) the residual temperature, Δt_r , the temperature remaining after the passage of the shock pulse, it also is a strong function of the shock pressure. 3) the strain induced temperature, ΔT_ε , that is the temperature resulting from the high rate deformation and appears, like the residual temperature, after the passage of the shock wave.

In powder compaction/consolidation this strain heat, as discussed in the earlier section on strain effects, has two components, the overall strain and the local strain associated with the deformation of the powder during the compaction process. Earlier investigations by [13] have reported that the shock properties "per se" are not a strong function of powder morphology or particle size based upon the work of [20,21]. These studies were done on spherical copper and iron powders that had a nominal order of magnitude difference in their average particle diameters, and found no differences in their Hugoniots. For these experiments, one must keep in mind that while the spherical particle sizes have changed, their relative packing densities are

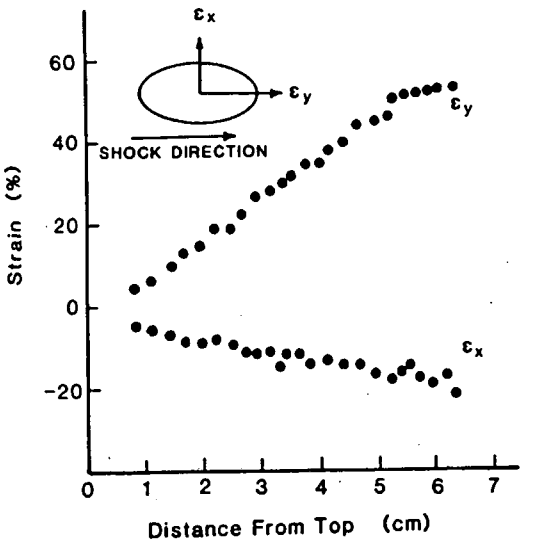

Figure 6. Measured strain in post shocked 304 stainless steel. The strain measurements are in the shock direction.

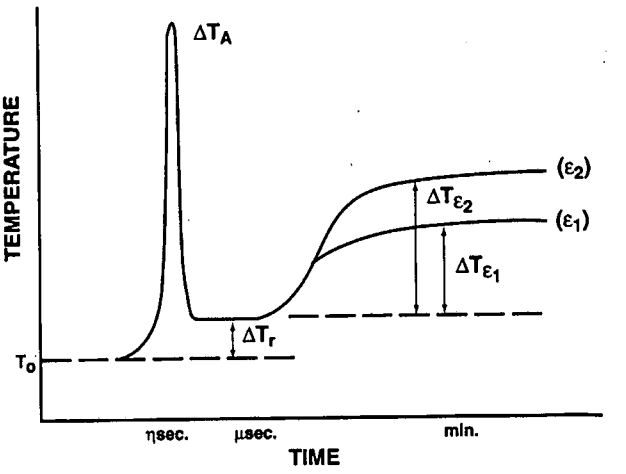

Figure 7. Schematic illustration of temperatures relative to the shock event. Where T_o is the ambient start temperature; ΔT_A, the shock adiabate temperature; ΔT_r, the residual temperature after passage of the shock and ΔT_ε, the strain induced temperature. Both ΔT_A and Δt_r are a function of the peak pressure, and ΔT_ε is a function of the strain magnitude at the shock strain rate (After XX).

unchanged. Thus, the distention's for each nominal size are unchanged. What in fact is different can best be illustrated in figure 8. Shown in figure 8 are schematic representations of ideal packing of mono-size (spherical) particles represented two-dimensionally. As the particle diameter decreases, the interstices (void space) between the spheres are correspondingly reduced. While the packing densities (ideally) are the same, the void volumes and distributions per interstitial site are much different. Thus, the temperature effects resulting from these different void volumes are directly related to the subsequent degree of deformation required to "fill" the void volume. For small mono-size spheres, the void volumes are small and consequently the deformation needed to "fill" the void space is small. This inherently requires less deformation than for large mono-size spheres. A consequence of this is the resultant temperature and its distribution within the shock consolidated monolith. This distribution can be visualized from the schematic illustrations shown in figure 9a and b. Figure 9a shows the effect of interstitial void volume vs. number of interstitial sites. The fewer interstitial sites, the greater the void volume and vice versa. Consequently, the greater the void volume, the greater the local particle strain needs to be to fill the interstitial void space. This is shown in figure 9b. Thus, for spherical geometry, the only particle size differences will range between local to distributive temperature effects within the compacted/consolidated monolith. This is schematically illustrated in figure 10. Thus, the temperature effect due to particle size alone will contribute to the residual temperature in a manner depicted schematically in figure 11.

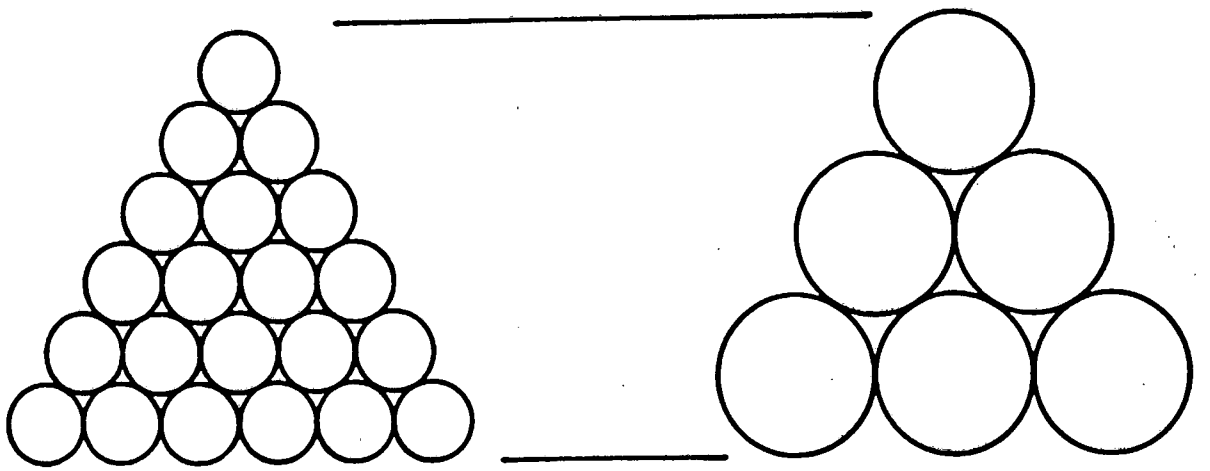

Figure 8. Ideal packing of monosize spherical particles schematically represented two-dimensionally. As the diameter is increased, the interstices (void volume) between spheres are correspondingly increased.

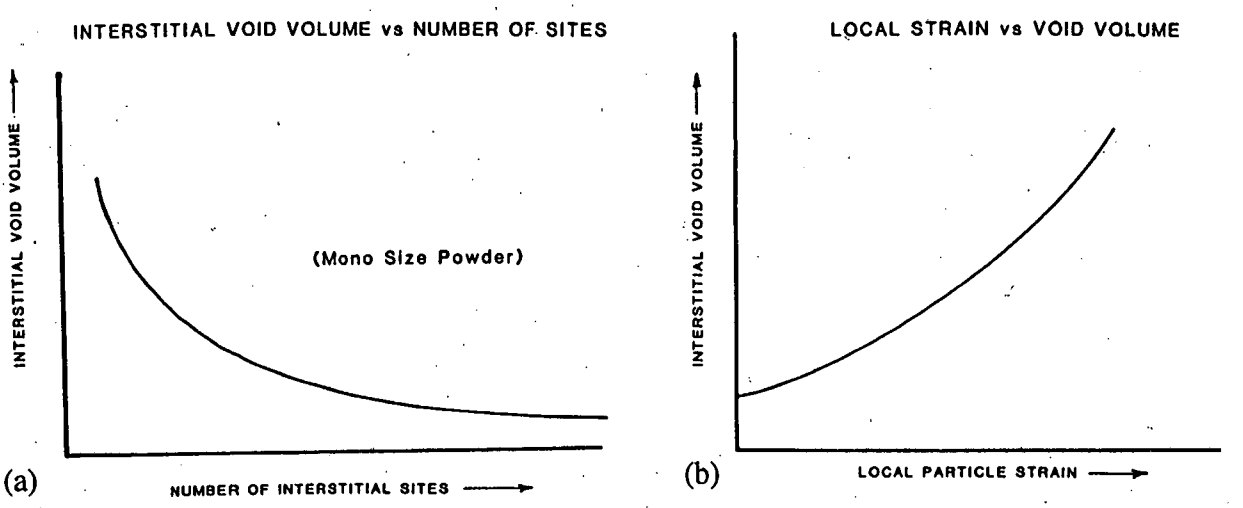

Figure 9. Interstitial void volume (from Fig. 8) versus number of sites for monosize powder (a), and local strain versus interstitial void volume (b).

This, in fact, alters the residual microstructure, particularly if melting occurs. As a consequence, the total temperature that a powdered sample "sees" over and above its ambient temperature, T_o, can be expressed as:

$$T_{Total} = T_o + [\Delta T_A + \Delta T_r + \Delta T_\varepsilon] \quad (4)$$

Where ΔT_ε can be expressed by its components $\Delta T_{overall\ \varepsilon} + \Delta T_{local\ \varepsilon}$. Thus, after the passage of the shock wave, ΔT_A approaches zero and the total RESIDUAL temperature from a shock event

is dominated by:

$$T_{\text{Total Residual}} = \Delta T_r + \Delta T_{\text{local }\varepsilon} \qquad (5)$$

The values for ΔT_r are tabulated for a number of metals and alloys in Table I and are given as a function of pressure [16]. The value for $\Delta T_{\text{overall }\varepsilon}$ is a function of the momentum trapping of the shock pulse and is material dependent; for stainless steel it has been experimentally determined and reported earlier [19] and was shown in figure 4. For other materials and shock designs, the $\Delta T_{\text{overall }\varepsilon}$ component must be determined experimentally via controlled strain experiments. The contribution of $\Delta T_{\text{local }\varepsilon}$ is controlled by the powder size and its distribution, as schematically illustrated in figure 11. The pressure profiles for a number of initial packing densities are shown in figure 12. These data were generated from a 2-D Eularian hydro-code in use at Los Alamos National Laboratory and proportionated to the densities given. A sample holder containing such powders is schematically illustrated in figure 13 and is typical of all of the post-shocked samples. One such typical cross-section is shown for a shocked RSR nickel based super alloy in figure 14. Although, this particular sample was overdriven by a large shock wave for compaction, it non-the-less illustrates all the regions discussed above. They include regions that contain compaction, consolidation, melt, Mach stem reactions as well as end plug alloying. In order to understand and interpret all of these regions, we need to profile the pressure-temperature and strain-temperature components first for a solid sample then for a sample containing powder. For 304 stainless steel, the P-T profile as generated from data such as that listed in Table I and given in reference 4 is shown in figure 15. Inherent in this figure are four distinct temperature regions that can be quantified by the amount of energy added to them by a given shock wave. Thus, by knowing their mass, specific heat and associated temperature rise

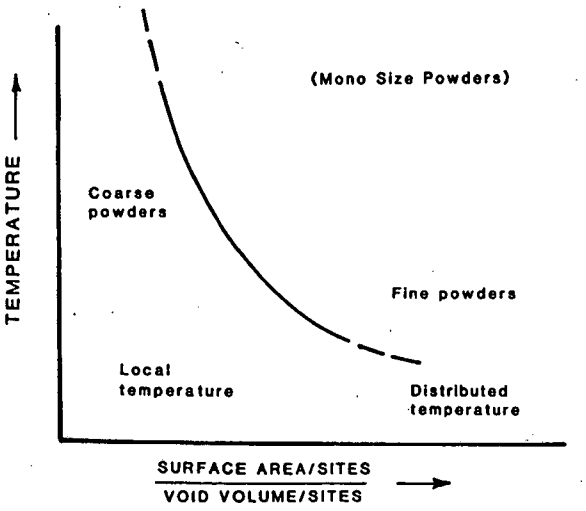

Figure 10. Temperature versus interstitial site distribution for monosize spherical powders. Site distribution is shown by the ratio of interstitial surface area/interstitial void volume (from Fig. 7).

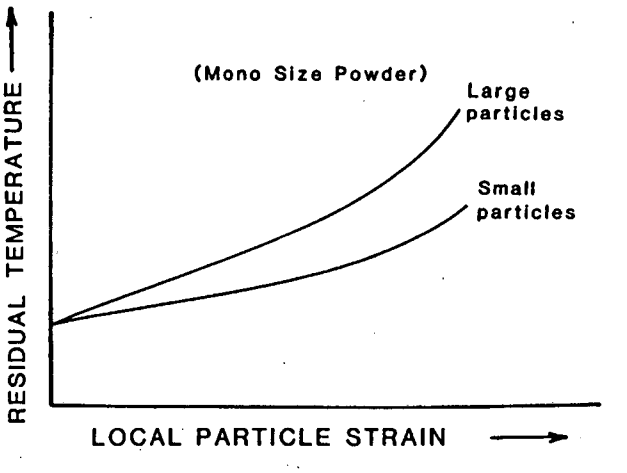

Figure 11. Ideal plot of residual temperature versus local particle strain to fill interstitial void space for large and small monosize spherical particle regimes.

Table 1. Thermodynamically Calculated Temperature Rises Produced by Shock Loading: ΔT_A-Temperature Rise at Hugoniot (Shock Front): ΔT_r-Temperature Rise after Passage (T_o at 390 K)

		Pressure (GPa)					
Material		10	20	30	40	50	60
Aluminum	ΔT_A	81	215	414	675	993	1361
(2024)	ΔT_r	15	74	169	288	422	565
Brass	ΔT_A	69	155	285	447	631	
Cobalt	ΔT_A	28	66	114	182	263	
Copper	ΔT_A	43	102	186	296	433	595
	ΔT_r	5	27	69	126	197	278
Iron	ΔT_A	50	123	228	364	527	714
	ΔT_r	9	45	105	183	275	376
Magnesium	ΔT_A	164	509	1021	1665	2418	3259
	ΔT_r	62	248	501	782	1067	1337
Molybdenum	ΔT_A	18	44	83	140	216	311
	ΔT_r	2	12	36	72	123	187
Nickel	ΔT_A	28	63	112	178	261	361
	ΔT_r	2	14	32	72	117	171
Niobium	ΔT_A	28	76	153	265	412	595
	ΔT_r	5	28	76	149	244	359
Rhenium	ΔT_A	20	44	75	117	171	237
	ΔT_r	1	7	19	40	68	105
Silver	ΔT_A	65	159	300	490	728	1009
	ΔT_r	10	51	123	218	329	450
Stainless	ΔT_A	39	89	159	251	366	502
Steel	ΔT_r	3	20	52	98	155	222
Tantalum	ΔT_A	26	68	134	229	355	511
	ΔT_r	4	22	61	121	201	299
Titanium	ΔT_A	10	113	242	421	644	906
	ΔT_r	9	53	134	248	386	541
Tungsten	ΔT_A	15	37	69	116	179	258
	ΔT_r	1	10	28	58	100	154

(ΔT), the quantity of heat can be calculated from, $Q = mc \quad \Delta T$. The four regions so represented are shown in figure 16, and the total energy input is the sum of these.

$$Q = Q_1 + Q_2 + Q_3 + Q_4 \tag{6}$$

By substituting a powdered sample in region Q_3, the highest temperature region, the deformation temperature (strain temperature, $\Delta T\varepsilon$) produced in the consolidation of this powder is thus added and quite often the samples melt. Consequently, the difference between the solid

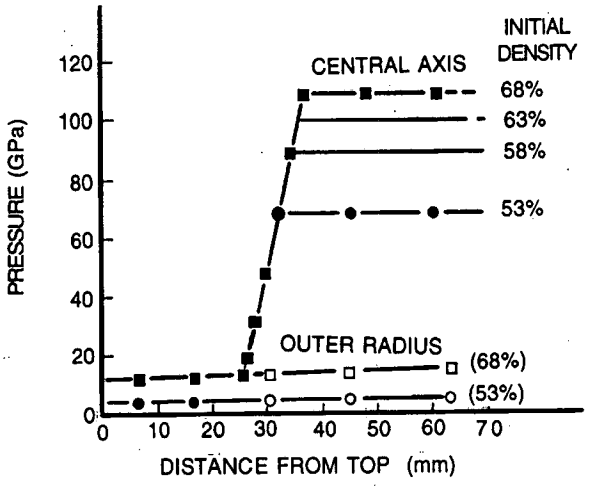

Figure 12. Hydro-code calculations of achieved pressure versus axial length as a function of initial density for 304 stainless steel powder.

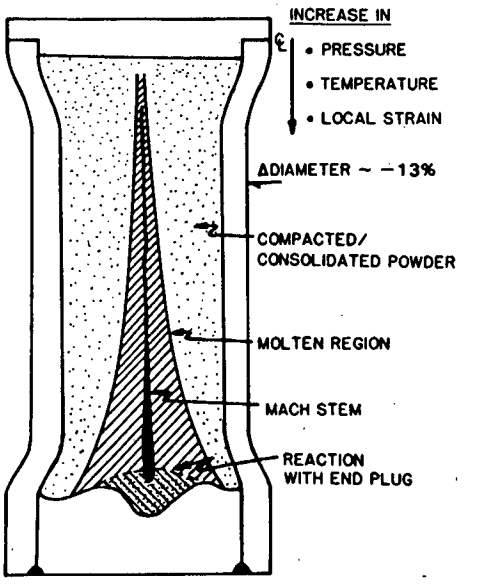

Figure 13. Schematic of post-shocked powder holder showing the various regions of interest.

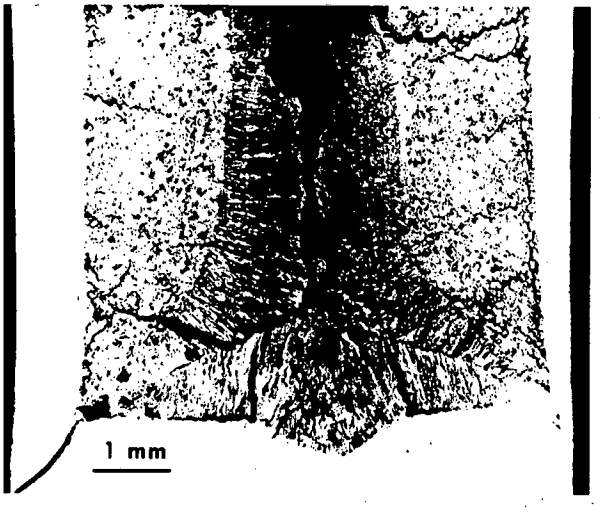

Figure 14. Cross-section of the lower portion of a shocked 304 stainless steel powder having an initial density of 68%.

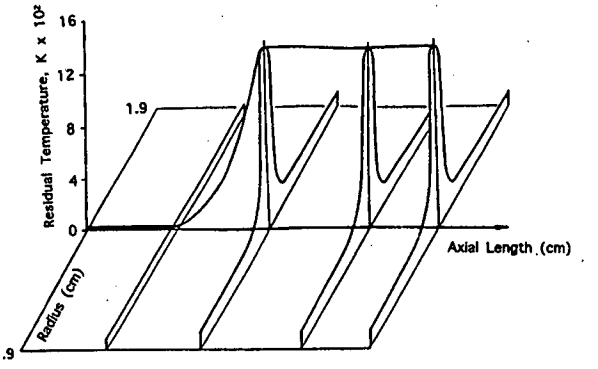

Figure 15. Radial and axial temperature profile of a solid cylindrically shocked 304 stainless steel sample.

sample and the one containing the powder can be measured via calorimetry shortly (~35 sec.) after the shock event. This has been described elsewhere [22]. For such an experiment, the resultant energy input (temperature) derived from the added strain from the compaction of the powder can schematically be seen in figure 17. Thus, by changing powder size and distribution

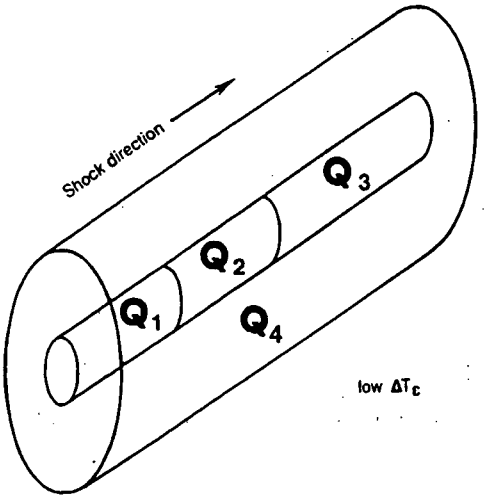

Figure 16. Schematic of shock sample showing regions under going known pressure regimes. The $Q_{1...4}$ designators refer to the heat input into the specific regions obtained from the temperature profile in Fig. 15.

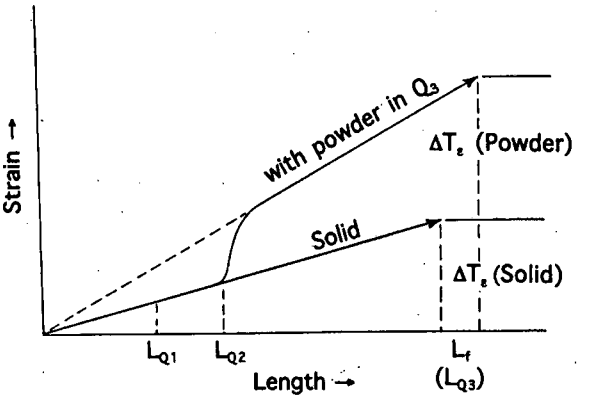

Figure 17. Schematic of the temperature distribution in the axisymmetric shock assembly for solid and powders contained within Q_3.

one can control the temperature through the deformation strain all the while keeping all else fixed. Results for such experiments on 304 stainless steel powders are shown in figure 18. Evident from this is the increased pressure required to consolidate without melting as a function of increased initial packing density. The lower pressure region of this figure shows the region where compaction is achieved. That is to say, near theoretical densities are obtained, however, the particles lack any large degree of bonding. At higher pressures but below the solid line is where good consolidation is achieved, with the best results achieved nearer the solid line. Above the solid line, particle melting is observed and is not desired for consolidation. At higher pressures bracketed by the dashed lines, the Mach stem region is observed. In shock processing to consolidate/fabricate components this region was to be avoided and/or eliminated by appropriately designing the shock system. However, it is within and near this region that perhaps some of our most interesting investigational observations have been obtained. In our attempt to better understand the deformation process to achieve optimal consolidation, the particle-to-particle deformation needed to be observed. To this end, the 304 stainless steel powder particles were platted with a very thin layer of gold. This allowed for inter-particle interfaces to be observed in the compaction/consolidation regions. However, as one approached the consolidation/melt region boundary, the gold became "alloyed" with the stainless steel powders. A radial cross-section of such a system is shown in figure 19. The gold alloying with the 304 stainless steel is first noticed in the consolidation region just adjacent to the melt region of figure 19 and can clearly be seen in the micrographs of figure 20. However, when one looks for the gold in the melt region, it is essentially uniformly distributed. With this observation, the mass transport rate of gold into the stainless steel powder can be calculated. Taking the average powder size of 122mm that the gold was distributed over and using the shock pulse width (pulse duration, ΔT) of 0.1 μs, obtained from the hydro-code calculations, a mass transport rate of 1220m/sec. is obtained. One must keep in mind that this occurs at a pressure of approximately 1

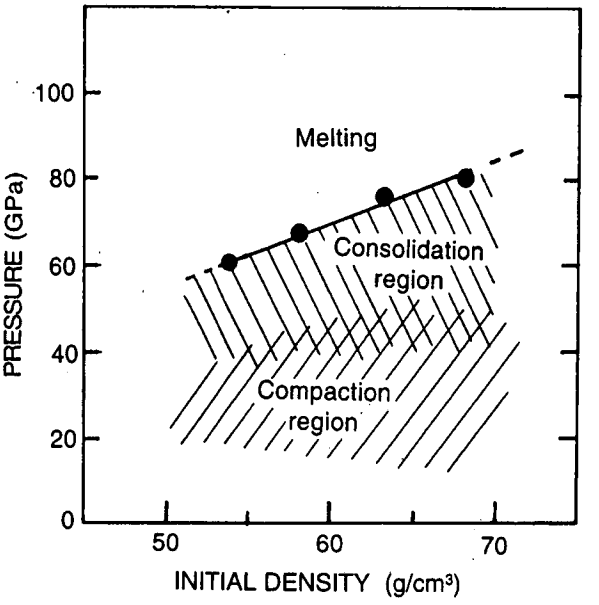

Figure 18. Pressure versus Initial density for304 stainless steel powders showing the regions for compaction, consolidation and melting. The dashed lines within the melt region bracket the Mach stem region.

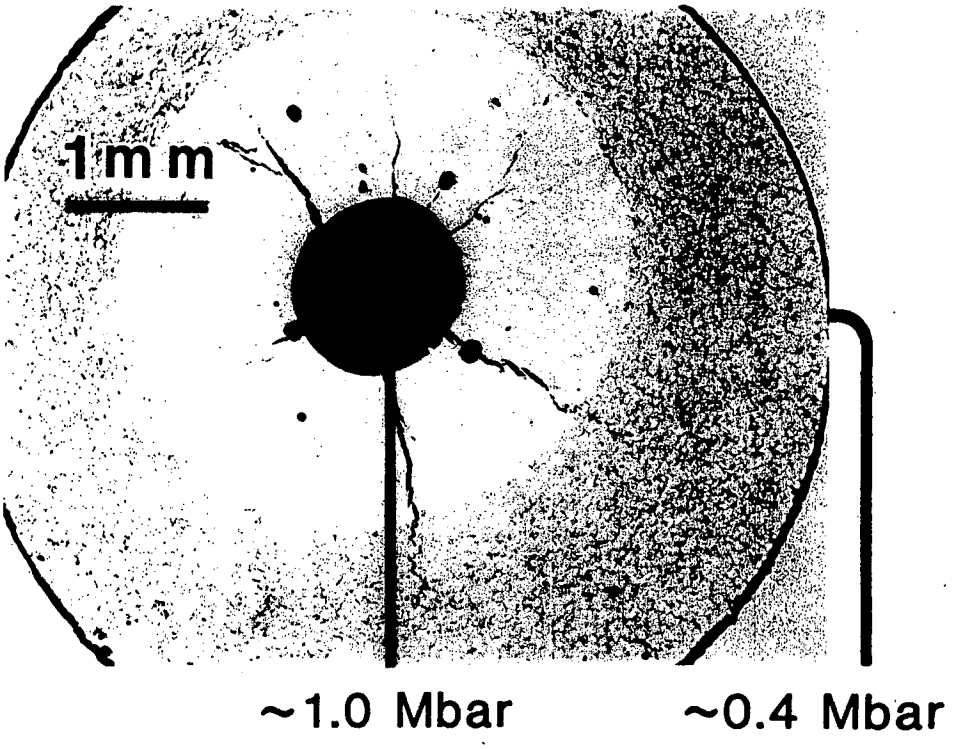

Figure 19. Cross-section of a 304 stainless steel gold-plated powder at 5.1 cm from the top of the sample. Pressure within the central axis ~100 GPa (~1 Mbar) and on the outer portion ~40 GPa (~ 0.4 Mbar).

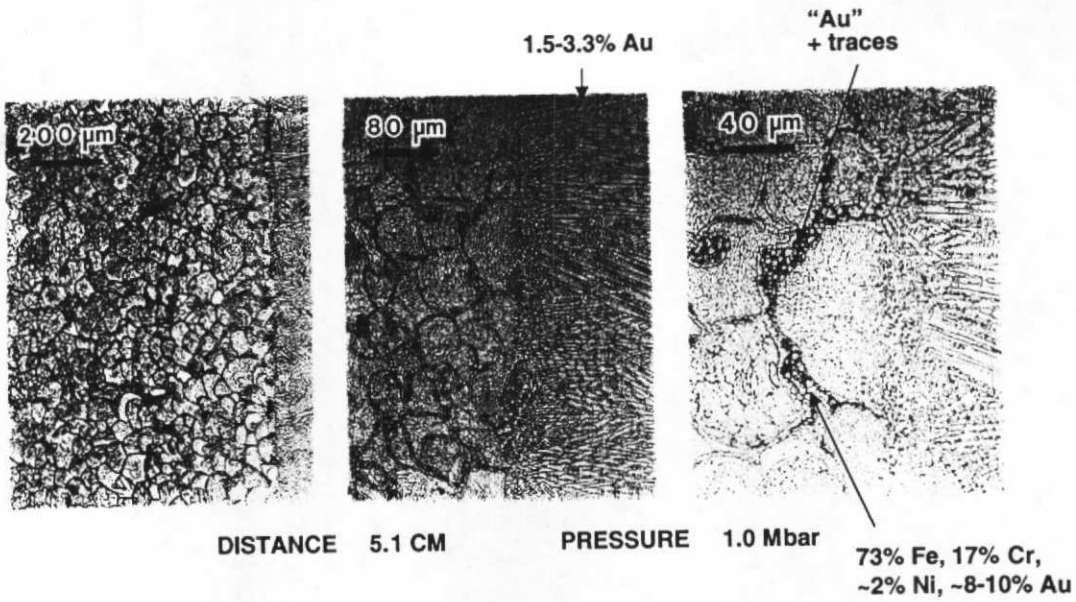

Figure 20. Micrographs taken at the transition zone between the consolidated and melt regions of Fig. 19. Compositional alloying can be observed around the particle interfaces. In the melt region the gold is in solution with the stainless steel. Mbar and a temperature in excess of 2000 K. Also that the sample is pressure and temperature quenched as the shock wave is removed by the momentum trap.

3. SUMMARY

In the discussions and illustrations given above some different explanations of the local thermal effects produced during shock processing of powders. Topic discussions were presented that covered the areas of compaction, consolidation and synthesis. Many of the earlier developed theories encompass parameters that account for the deposition of energy (temperature) uniformly on the outer surface of each particle. From the micrographs shown in figures 19 and 20, it is clear that melting where it occurred was localized and occurred at regions of greatest strain (the deformation to fill the void) within the consolidated region, and totally melted within the Mach stem region. While this is undesirable for shock compaction and consolidation, it indeed can be used for synthesis and metastable alloying. Using this axisymetrical shock method as an investigational technique allows for the opportunity to screen a large number of alloy systems within a pressure-temperature regime here-to-for unobtainable previously.

ACKNOWLEDGMENTS

The author would like to acknowledge the contributions of W. J. Medina, LANL for the experimental support and for the many colleagues far and wide, for the numerous constructive discussions. The DOE under contract W-7405-ENG-36, in part, supported this work.

REFERENCES

[1] Linse, V., Chairman, National Materials Advisory Board, *"Dynamic Compaction of Metal and Ceramic Powders,"* NMAB-394, (National Academic Press, Washington, DC, 1983).

[2] Gourdin, W.H., *"Dynamic Consolidation of Metal Powders,"* Progress in Materials Science, 30, (1986), 39.

[3] Thadhani, N.N., *"Shock Compression Processing of Powders,"* Adv. Matl. & Manufac. Proc., 3(4), (1988), 493.

[4] Duvall, G.E. and Graham, R.A., *"Phase Transitions Under Shock Wave Loading,"* Rev. Mod. Phys., 49, (1977), 523.

[5] Al'tshuler, L.V., *"Phase Transitions in Shock Waves (Review),"* translated from Zhurnal Prikladnoi Mekhaniki I Technicheskoi Fizki, No. 4, (1978), pp. 93-103.

[6] DeCarli, P.S. *"Method of Making Diamond,"* U.S. Patent No. 3,238,019, March 1, 1966.

[7] DeCarli, P.S. and Jamieson, J.C., *"Formation of Diamond by Explosive Shock,"* Science, 133, (1961), 1821.

[8] DeCarli, P.S. and Milton, D.J., *"Stishovite: Synthesis by Shock Wave,"* Science, 147, (1965), 144.

[9] Ryabinin, Yu.M., *"Certain Experiments on Dynamic Compression of Substances,"* Soviet Phys. Tech., Phys., 1, (1956), 2575.

[10] Dremin, A.N. and Bruesov, O.N., *"Processes Occurring in Solids Under the Action of Powerful Shock Waves,"* Russian Chemical Reviews, 37-5(1968), 392.

[11] Duvall, G., Chairman *"Shock Compression Chemistry in Materials Synthesis and Processing,"* National Materials Advisory Board, NMAB-414, National Academy Press, Washington, DC, 1984.

[12] Graham, R.A., Morosin, B., Venturini, E.L. and Carr, M.J., *"Materials Modification and Synthesis Under High Pressure Shock Compression,"* Ann. Rev. Mater. Sci., 16 (1986), 315.

[13] Gourdin, W.H., *"Dynamic Consolidation of Metal Powders,"* Progress in Materials Science, 30 (1986), 39-80.

[14] Murr, L.E., *Shock Waves for Industrial Applications*, (Park Ridge, New Jersey:Noyes Publications, 1988), 237.

[15] McQueen, R.G., et al., *High-Velocity Impact Phenomena* (New York, NY:Academic Press, 1970), 293.

[16] Appendix B in *Shock Waves and High-Strain-Rate Phenomena in Metals-Concepts and Applications*, Ed. by Meyers M.A., and Murr, L.E., (New York, NY:Plenum Press, 1980), 1041.

[17] Follansbee, P.S. *"High-Strain-Rate Deformation of FCC Metals and Alloys"* in *Metallurgical Applications of Shock-Wave at High-Strain-Rate Phenomena*, Eds. L.E. Murr, K.P. Staudhammer and M.A. Meyers, (New York, NY:Marcel Dekker, Inc., 1986), 451.

[18] Johnson, K.A., Murr, L.E. and Staudhammer, K.P., *"Comparison of Residual Microstructures for 304 Stainless Steel Shock Loaded in Plane and Cylindrical Geometries: Implications for Dynamic Compaction and Forming,"* Acta Met., 33 (1985), 677.

[19] Johnson, K.A., and Staudhammer, K.P., *High-Strain-Rate ~10 ^{6}/s Response of 304 Stainless Steel at various Strains*, in *Metallurgical Applications of Shock-Wave at High-Strain-Rate Phenomena*, Eds. Murr, L.E., Staudhammer, K.P., and Meyers, M.A., (New York, NY:Marcel Dekker, Inc. 1986), 525.

[20] Boade, R.R., *"Principal Hugonoit, Second Shock Hugonoit, and Release Behavior of Pressed Copper Powder,"* J.Appl. Phys. 41, (1970), 4542-4551.

[21] Butcher, B.M., and Karnes, C.H., *"Dynamic Compaction of Porous Iron,"* J. Appl. Phys. 40, (1969), 2967-2976.

[22] Staudhammer, K.P., "*Measurement of Residual Temperatures in Shock-Loaded Cylindrical Samples of 304 Stainless Steel*, in Shock-Waves and High-Strain-Rate Phenomena in Materials", Ed. by Meyers, M.A., Murr, L.E., and Staudhammer, K.P., (New York, NY:Marcel Dekker, Inc. 1992), 971-980.